LAWRENCE
LIVERMORE
NATIONAL
LABORATORY

Detailed chemical kinetic oxidation mechanism for a biodiesel surrogate

O. Herbinet, W. J. Pitz, C. K. Westbrook

September 24, 2007

Combustion and Flame

Detailed chemical kinetic oxidation mechanism for a biodiesel surrogate

Olivier Herbinet, William J. Pitz and Charles K. Westbrook

Lawrence Livermore National Laboratory, California 94550, USA

Full-length article

Corresponding author:

William J. Pitz
Lawrence Livermore National Laboratory
7000 East Avenue
Mail Stop L-372
Livermore, CA 94550
Tel: 925 422 7730
Fax: 925 424 4334
E-mail: pitz1@llnl.gov

Detailed chemical kinetic oxidation mechanism for a biodiesel surrogate

Olivier Herbinet, William J. Pitz and Charles K. Westbrook

Lawrence Livermore National Laboratory, California 94550, USA

Abstract

A detailed chemical kinetic mechanism has been developed and used to study the oxidation of methyl decanoate, a surrogate for biodiesel fuels. This model has been built by following the rules established by Curran et al. for the oxidation of n-heptane and it includes all the reactions known to be pertinent to both low and high temperatures. Computed results have been compared with methyl decanoate experiments in an engine and oxidation of rapeseed oil methyl esters in a jet stirred reactor. An important feature of this mechanism is its ability to reproduce the early formation of carbon dioxide that is unique to biofuels and due to the presence of the ester group in the reactant. The model also predicts ignition delay times and OH profiles very close to observed values in shock tube experiments fueled by n-decane. These model capabilities indicate that large n-alkanes can be good surrogates for large methyl esters and biodiesel fuels to predict overall reactivity, but some kinetic details, including early CO_2 production from biodiesel fuels, can be predicted only by a detailed kinetic mechanism for a true methyl ester fuel. The present methyl decanoate mechanism provides a realistic kinetic tool for simulation of biodiesel fuels.

Keywords

Methyl decanoate, oxidation, biodiesel fuels, kinetic modeling, engine, low temperature

Introduction

In recent years, biodiesel has become interesting as an additive to diesel fuel for two main reasons. This renewable alternative fuel can reduce dependence on imported petroleum and can also contribute to environment preservation by lowering net emissions of greenhouse gases. The use of biodiesel in diesel engine decreases emissions of pollutants such as carbon monoxide, unburned hydrocarbons and particulate matter, although a slight increase in emissions of nitrogen oxides is observed in some cases [1-4].

Biodiesel is a multiple component mixture of mono-alkyl esters of long-chain fatty acids derived from vegetable oils and animal fats. Most biodiesel fuels used in the world are made from soy oil and rapeseed oil by transesterification with an alcohol. The soy and rapeseed derived biodiesels are complex mixtures composed of mainly five saturated and unsaturated methyl esters (when methanol is used for the transesterification process): methyl palmitate ($C_{17}H_{34}O_2$), methyl stearate ($C_{19}H_{36}O_2$), methyl oleate ($C_{19}H_{34}O_2$), methyl linoleate ($C_{19}H_{32}O_2$) and methyl linolenate ($C_{19}H_{30}O_2$). Average compositions of soybean and rapeseed biodiesels [5] are given in Table 1.

Table 1

The structures of these components are displayed in Figure 1, showing the considerable structural similarities in these chemical species, each with a methyl ester attached to a large hydrocarbon fragment.

Figure 1

Very few kinetic studies of biodiesel fuel combustion have been carried out, either experimentally or using computational modeling. There are several reasons for this lack of attention; biodiesel fuels have become important only quite recently, and they are generally very large fuel molecules that challenge the capabilities of kinetic modeling. As a result, past research in this area has followed two major paths. Experiments and kinetic modeling of much smaller methyl esters have addressed the special features of methyl ester oxidation, and combustion of large biofuels has been studied by assuming that large methyl esters can be approximated as being fundamentally the same as large n-alkanes. The largest methyl ester that has been studied kinetically is methyl butanoate, with a chain of only 4 carbon atoms connected to the methyl ester group. Kinetic modeling of methyl butanoate has concluded that this fuel reproduces kinetic features of the oxidation of the methyl ester but does a poor job of reproducing kinetic features of diesel fuels with their chains of 16 - 18 carbon atoms. Other studies have used kinetic models for n-alkanes as large as n-hexadecane to simulate the combustion of the large methyl ester molecules in actual biodiesel fuels. The present work is intended to provide a reliable kinetic model for a methyl ester fuel that is much larger than the previous methyl butanoate. Instead of the 4 carbon atoms chain of methyl butanoate, the current

work provides a kinetic mechanism for methyl decanoate (cetane number of about 47 [6,7]), with a chain of 10 carbon atoms with a methyl ester group attached (Figure 1). Methyl decanoate reacts in a manner that is much closer to actual biodiesel fuel than methyl butanoate, including both early production of CO_2 from the methyl ester group and burning in a manner very similar to conventional diesel fuel.

We will review past work in the area of methyl ester combustion, leading to a description of the goals of the present work.

The oxidation of methyl butanoate ($C_5H_{10}O_2$) has been the subject of several papers. A detailed chemical kinetic mechanism for the combustion of methyl butanoate was developed by Fisher et al. [8], which was validated against the limited available data obtained at low temperature, subatmospheric conditions in closed vessels, using pressure measurements as the main diagnostic. More recently, Metcalfe et al. [9] studied the oxidation of methyl butanoate and ethyl propanoate in a shock tube. A revised detailed kinetic mechanism based on the work of Fisher et al. [8] for methyl butanoate and a new submechanism for ethyl propanoate were used to simulate measured ignition delay times with good agreement. Gaïl et al. performed a wide-ranging kinetic modeling study of the oxidation of methyl butanoate [10]. They obtained experimental species profiles in a jet stirred reactor, a variable pressure flow reactor and an opposed-flow diffusion flame. A revised kinetic model based on the Fisher et al. mechanism was validated from the jet stirred reactor data. This model was shown to reproduce data obtained in a variable pressure flow reactor and in an opposed-flow diffusion flame. Sarathy et al. [11] performed an experimental study of methyl crotonate ($C_5H_8O_2$ unsaturated methyl ester) in a jet stirred reactor and an opposed-flow diffusion flame in order to compare with

experimental data obtained for methyl butanoate [10] and understand the role of the double bond in the methyl ester.

Vaughn et al. [12] studied the combustion of bio-ester fuel droplets in microgravity. They measured ignition time of neat methyl esters (such as methyl butanoate, methyl decanoate, methyl dodecanoate, and methyl oleate) and commercial soy oil methyl esters. Ignition delay times obtained during this study showed that methyl decanoate and methyl dodecanoate are better surrogates for commercial soy oil methyl esters than methyl butanoate, in agreement with conclusions of Fisher et al. [8] and Gaïl et al. [10].

Dagaut et al. [13] performed an experimental study of the oxidation of rapeseed oil methyl ester (RME) in a jet stirred reactor at 1-10 atm over the temperature range 800-1400 K. Experimental species profiles were compared with computed mole fractions from a mechanism for oxidation of n-hexadecane, which had been validated against experiments in a JSR [14]. The agreement was shown to be satisfactory and n-hexadecane appeared to be a good surrogate for rapeseed oil methyl ester in the conditions of the study. However, the n-hexadecane mechanism was unable to predict the early production of CO_2 which was observed in the experiments. More recently Dagaut and Gaïl studied the oxidation of a blend of Jet-A1 and RME (80/20, mol/mol) in a jet stirred reactor [15]. Experiments have been performed at a pressure of 10 atm, a residence time of 0.5 s and at an equivalence ratio of 1. The formation of unsaturated methyl esters (methyl-2-propenoate, methyl-3-butenoate, methyl-4-pentenoate and methyl-5-hexenoate) has been observed in this study. Pedersen et al., who performed a qualitative study of the species from the oxidation of rapeseed oil methyl esters in a

stainless steel tubular reactor at 823 K, have also observed the formation of unsaturated species: methyl-2-propenoate, methyl-3-butenoate, methyl-5-hexenoate and methyl-6-heptenoate. The formation of methyl-4-pentenoate has not been observed [16].

A good knowledge of the kinetics of the reaction of biodiesel fuels at both high and low temperature is necessary to perform reliable simulations of ignition, combustion and emissions in homogeneous charge compression ignition (HCCI) and diesel engines. Modeling of the oxidation of methyl butanoate provided a better understanding of the chemistry of methyl esters combustion, but methyl butanoate is not a good surrogate for commercial biodiesel fuels because its alkyl chain is too short. In this work, a detailed chemical kinetic mechanism has been developed and used to study the oxidation of methyl decanoate, which we feel is a much better surrogate for biodiesel fuel than methyl butanoate. This model is compared with the limited available experimental data obtained in a motored engine [17,18], and it is used to model rapeseed oil methyl ester experiments in a JSR [13] and shock tube ignition of n-decane [19].

Description of the chemical kinetic mechanism

The detailed chemical kinetic mechanism of the oxidation of methyl decanoate has been developed by using the same systematic rules which have been described by Curran et al. for n-heptane and iso-octane [20,21]. Some kinetic parameters and thermochemical properties used in this mechanism have been updated from more recent data from the literature. The entire mechanism will be available, including the kinetic parameters and thermochemistry, in Chemkin format on our web page at:

http://www-cmls.llnl.gov/?url=science_and_technology-chemistry-combustion

Description of the methyl decanoate kinetic chemical mechanism

The model presented in this paper was developed from previous n-heptane and iso-octane [20,21] and methyl butanoate mechanisms [8] by combining them with the low and high temperatures chemistry specific to methyl decanoate. The overall primary oxidation reaction pathways in the methyl decanoate mechanism are shown in Figure 2. The same general pathways apply to all hydrocarbon fuels, although the details of each step depend on the size and structure of the specific fuel being studied. In general, the reaction classes from Curran et al. were used, but accommodations were required to take into account the fact that the methyl ester group in methyl decanoate changes some of the details of the mechanism.

Figure 2

High temperature part. At high temperatures, unimolecular decompositions of the fuel and H-atom abstractions from the fuel lead to the formation of alkyl and alkyl-ester radicals. Reactions of these radicals, which are known to be pertinent at high temperature, are isomerizations, decompositions to olefins or unsaturated esters plus smaller radicals, and direct abstractions by O_2 to olefins or unsaturated esters plus HO_2. Olefins and unsaturated esters formed through these primary routes react in turn through the same types of reactions as the fuel and through other reactions specifically due the presence of the double bond (additions of radicals to the double bond, decomposition by retro-ene reactions).

8

The unimolecular initiation reactions of methyl decanoate were written in the recombination direction and the kinetic parameters for the decomposition direction were then calculated using the thermodynamic properties. A rate constant of 1.0×10^{14} $cm^3.mol^{-1}.s^{-1}$ was used for the recombination of an H atom and any C_{11} ester radical, 3.0×10^{13} $cm^3.mol^{-1}.s^{-1}$ for the two reactions of recombination involving C-O bonds, 1.8×10^{13} $cm^3.mol^{-1}.s^{-1}$ for the recombination leading to the formation of the C-CO bond, 3.0×10^{13} $cm^3.mol^{-1}.s^{-1}$ for the formation of the C-C bond involving a methyl radical and an alkyl-ester radical, and 8.0×10^{12} $cm^3.mol^{-1}.s^{-1}$ for the remaining C-C bonds formed through the reactions of recombination of alkyl and alkyl-ester radicals. Reactions of recombination involving C-C and C-O bonds in methyl decanoate are shown in Table 2.

Table 2

H-atom abstractions from methyl decanoate by H, CH_3, C_2H_3, C_2H_5, O, O_2, OH, HO_2, CH_3O, and CH_3O_2 have been included, using kinetic parameters recommended by Curran et al. [20]. Distinctions between three types of H atoms were made: primary H atoms in the two methyl groups at each end of the molecule, secondary H atoms bonded to the conventional secondary, internal carbon atoms, and the two H atoms bonded to the carbon atom adjacent to the carbonyl group. There is a lack of data concerning the rate constants of H-atom abstractions involving these two H atoms. These H atoms have C-H bond energies similar to those for tertiary C-H bonds, so we have followed [8] and used H atom abstraction rates from tertiary bonds in other molecules for these H atoms.

Alkyl and alkyl-ester radical decompositions were written in the reverse direction (addition of a radical to a double bond). Kinetic parameters are based on a recent review by Curran for the alkyl radicals [22] and from the methyl butanoate mechanism [8] for reactions involving atoms of the ester group. The kinetic parameters for addition of radicals to the oxygen of the C=O bond have been updated from the study of methyl radical addition to the C=O bond by Henry et al. [23]. Kinetic parameters used for isomerizations, or H-atom shifts, of radicals were taken from quantum calculations performed by Matheu et al. [24]. Some required rate constants not calculated by these authors are estimated using "structure-reactivity" relationships. The rate constant used for the direct abstraction from alkyl and alkyl-ester radicals by O_2 is $1.6 \times 10^{12} \times exp[-5000(cal.mol^{-1})/RT]$ $cm^3.mol^{-1}.s^{-1}$ [25].

As far as olefins and unsaturated esters are concerned, H-atom abstractions and molecular decompositions by retro-ene reactions were written in a systematic way. Rate constants for primary, secondary and tertiary H-atoms abstractions from olefins and unsaturated esters are the same as those described above for the methyl decanoate molecule. For allylic and vinylic H-atoms, kinetic parameters are those recommended by Curran et al. [20] for small species (propene, 1-butene). The rate constant for the molecular decomposition of olefins and unsaturated esters by retro-ene reaction is from King [26]: $3.98 \times 10^{12} \times exp[-57630(cal.mol^{-1})/RT]$ s^{-1}. Only unimolecular initiations involving C-C and C-H bonds in the beta position of the double bond have been taken in account. Other C-C, C-O and C-H bond breakings were not included because of their higher activation energies. Unimolecular decompositions of olefins and unsaturated esters by scission of the allylic C-C bond were written in the forward direction and the scission

of the allylic C-H bonds in the reverse, recombination direction. Rate constants of $2.5 \times 10^{16} \times \exp[-71000(\text{cal.mol}^{-1})/RT]$ s^{-1} and 1.0×10^{14} cm^3.mol^{-1}.s^{-1} [20] were used, respectively. Additions of OH radicals to the double bond of olefins and unsaturated radicals were written (rate constants of $1.129 \times 10^5 \times T^{2.28} \times \exp[1241(\text{cal.mol}^{-1})/RT]$ cm^3.mol^{-1}.s^{-1} from Zhu et al. [27]) and additions of H atoms and HO$_2$ radicals were considered in two other parts of the mechanism (alkyl and alkyl-ester radicals C-H β-scission decompositions in the high temperature part and QOOH C-O β-scission decompositions in the low temperature part).

Rate constants for isomerizations of alkenyl, allylic and vinylic radicals are from [24]. Decompositions of these radicals were considered through the reverse additions and kinetic parameters are the same as those presented in the methyl decanoate section above.

Low temperature part. The low temperature part of the mechanism was built by adapting the kinetic scheme used in the well-validated n-heptane and iso-octane mechanisms. Again, some accommodations were required due to the presence of the methyl ester group in the fuel. Figure 3 displays a potential energy diagram (derived from the n-heptane and iso-octane mechanisms [20,21]) showing the major species and the main reaction pathways involved in the low temperature part of the methyl decanoate mechanism.

Figure 3

The first step of the low temperature mechanism is the addition of alkyl and alkyl-ester radicals to O_2 (Figure 4). Rate constants of 4.52×10^{12} $cm^3.mol^{-1}.s^{-1}$, 7.54×10^{12} $cm^3.mol^{-1}.s^{-1}$ and 1.41×10^{13} $cm^3.mol^{-1}.s^{-1}$ were used for additions of primary, secondary and tertiary radicals to O_2. The subsequent alkyl and alkyl-ester peroxy radicals (RO_2) react then by isomerizations to hydroperoxy alkyl and hydroperoxy alkyl-ester radicals (QOOH). Isomerizations through 5, 6, 7 and 8 member cyclic transition states have been included (Figure 5). Rate constants for isomerizations are from Curran et al. [21] and are presented in Table 3.

Figure 4

Figure 5

Reactions of hydroperoxy alkyl and hydroperoxy alkyl-ester radicals (QOOH) are displayed in Figure 6, including the second addition of O_2 forming hydroperoxy peroxy radicals (O_2QOOH), the decomposition to cyclic ethers plus OH, and the C-O β-scission decomposition to HO_2 and alkyl or alkyl-ester radicals. Other reactions of C-C β-scissions have not been taken in account because of their higher activation energy [28]. Rate constants for QOOH decompositions to cyclic ethers plus OH and to olefin plus HO_2 are those recommended by Curran et al. [20] (Table 3). The rate expression of the last reaction type is written as the reverse addition of olefin + HO_2, with different activation energies depending on whether the HO_2 adds to a primary or secondary carbon

atom. The direct eliminations from RO_2 (leading to olefins + HO_2) which intervenes in the more recent scheme proposed for the low temperature of alkyl radicals [28-30] were not included in the methyl decanoate mechanism and were also not included in the n-heptane and iso-octane mechanisms on which it is based. When developing these mechanisms it was believed that the channel of formation of olefins plus HO_2 occurred via C-C β-scissions following isomerizations through 5 member ring and kinetic parameters of these and related reactions were calibrated to reproduce the formation of olefins. Reaction rate rules for direct elimination of HO_2 from RO_2 in concert with RO_2 isomerizations need to be derived and validated for lower molecular weight systems where much more experimental data is available before they can be successfully applied to high molecular weight systems like the present work. We anticipate that future revisions of the present mechanism may address this direct molecular elimination reaction pathway, but the present mechanism represents an internally consistent and predictive modeling tool in its present form.
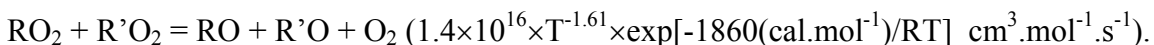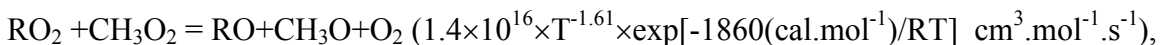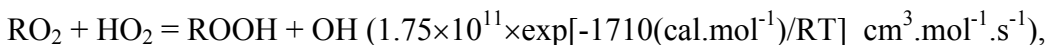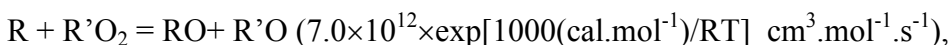
Figure 6

For O_2QOOH species, only those specific isomerizations leading to ketohydroperoxide plus OH have been included (Figure 7). Other isomerizations described as "alternative paths" by Silke et al. [31], have not been included and are not expected to be significant for long, straight chain hydrocarbons such as n-alkanes or the straight-chain methyl esters such as methyl decanoate, both of which have many possible paths for ketohydroperoxide + OH production. Kinetic parameters for O_2QOOH

isomerizations (producing ketohydroperoxide + OH) are derived from the rate constants for RO_2 isomerizations to QOOH, using the same A factors and activation energies 3 kcal.mol^{-1} smaller than for the analogous RO_2 isomerizations [20,21].

Figure 7

Decomposition reactions of ketohydroperoxides lead to the formation of a new OH radical and another radical, providing chain branching, following reaction type 24 from Curran et al.. The rate of hydroperoxide decomposition (O-O scission) used in the mechanism is $1.05 \times 10^{16} \times exp[-41600(cal.mol^{-1})/RT]$ s[-1] [32]. The following reactions of disproportionation between radicals have been included with rate expressions suggested by Curran et al. [20,21]:

$R + R'O_2 = RO + R'O$ ($7.0 \times 10^{12} \times exp[1000(cal.mol^{-1})/RT]$ cm^3.mol^{-1}.s^{-1}),

$RO_2 + HO_2 = ROOH + OH$ ($1.75 \times 10^{11} \times exp[-1710(cal.mol^{-1})/RT]$ cm^3.mol^{-1}.s^{-1}),

$RO_2 + CH_3O_2 = RO + CH_3O + O_2$ ($1.4 \times 10^{16} \times T^{-1.61} \times exp[-1860(cal.mol^{-1})/RT]$ cm^3.mol^{-1}.s^{-1}),

$RO_2 + R'O_2 = RO + R'O + O_2$ ($1.4 \times 10^{16} \times T^{-1.61} \times exp[-1860(cal.mol^{-1})/RT]$ cm^3.mol^{-1}.s^{-1}).

The above described mechanism involves 3012 species and includes 8820 reactions. The high numbers of reactions and species are caused by the numerous types of reactions taken in account but also to the fact that methyl decanoate is not a symmetric molecule like an n-alkane. Isomerizations of RO_2 species in the low temperature regime are also responsible for the large increase in the number of reactions because of the numerous permitted H-shifts.

Table 3

Thermodynamic properties

Standard enthalpies of formation, entropies and specific heats of the molecules and radicals involved in the mechanism have been calculated using the THERM program developed by Ritter and Bozzelli [33]. This program is based on the group and bond additivity methods proposed by Benson [34].

The C-H bond dissociation energy of the carbon atom adjacent to the carbonyl group has been updated from the recent work of El-Nahas et al. [35] who studied the thermochemistry of methyl butanoate by performing quantum calculations. The value used in the mechanism for this specific bond is 94.1 kcal.mol^{-1}. This compares closely to tertiary bond dissociation energies (96.5 kcal.mol^{-1}) as noted above for H atom abstractions from this site in methyl decanoate.

Results and discussion

A detailed kinetic mechanism is incomplete without a validation study comparing computed results from the mechanism with measurements from appropriate experiments. In many cases, laboratory experiments from shock tubes, laminar flames, stirred and flow reactors, and many other idealized systems are available, as well as experiments in engines or other practical systems. The laboratory experiments are especially valuable when they provide species-dependent and time-dependent information that provide a particularly demanding test of a mechanism, in contrast with experiments that provide

only an integrated test, such as an ignition delay time or laminar burning velocity. In the present case of methyl decanoate, however, we could not identify any fundamental laboratory experiments using methyl decanoate, and only one engine experiment was found that specifically used methyl decanoate as a fuel.

As a result, we have been able only to compare computed results for methyl decanoate combustion with experimental results for two closely related fuels, n-decane, for which we have used experimental results from low and high temperatures shock tube experiments, and rapeseed oil methyl ester, for which we have used experimental results from a jet-stirred reactor. Finally, we compared computed results with experimental data obtained in a motored engine [17,18], which used methyl decanoate as a fuel, in addition to other cases using n-heptane and commercial diesel fuel.

Comparison with rapeseed oil methyl esters jet stirred reactor experiments

Dagaut el al. [13] studied oxidation of rapeseed oil methyl ester (RME) in a jet stirred reactor (JSR) at pressures of 1 and 10 atm, at temperatures from 800 to 1400 K and at several residence times (0.07, 0.1 and 1s) and equivalence ratios (0.25 − 1.5). Quantification of the species leaving the reactor was performed by gas chromatography (FID, TCD) and a GC/MS was used for their identification. Quantified species were 1-alkenes from ethylene to 1-heptene, methane, hydrogen, carbon dioxide, carbon monoxide and oxygen. Dagaut et al. did not report any data about the formation of unsaturated methyl esters in this paper. The formation of these species, with a double bond at the extremity of the hydrocarbon chain, is expected because they can be obtained via the same routes than the above mentioned 1-olefins. More recently, the formation of

unsaturated methyl esters has been observed by Dagaut and Gaïl during the study of the oxidation of a blend of Jet-A1 and RME (80/20, mol/mol) in a jet stirred reactor [15]. Four unsaturated esters have been identified in the study: methyl-2-propenoate, methyl-3-butenoate, methyl-4-pentenoate and methyl-5-hexenoate.

Two sets of simulations have been performed to draw comparisons with data performed at 10 atm (approximating pressures met in engines): first by using neat methyl decanoate as surrogate and second by using a surrogate composed of methyl decanoate and n-heptane. The choice of this last surrogate is justified later in the paper.

JSR simulations with neat methyl decanoate. Methyl decanoate ($C_{11}H_{22}O_2$) is a smaller molecule than those found in rapeseed oil methyl esters (global formula of $C_{17.92}H_{33}O_2$ from [13]). Therefore, the experimental inlet mole fraction of RME (0.005) has been multiplied by a factor 18/11 in order to match the inlet flux of carbon atoms in rapeseed oil methyl esters. This leads to slightly higher numbers of H- and O-atoms in our C_{18} surrogate: 36 and 3.27 respectively, compared with 33 and 2 in RME. Inlet oxygen mole fractions were deduced from the values used by Dagaut et al. for their simulations with n-cetane. These values were reduced slightly in order to take in account the presence of oxygen atoms in methyl decanoate. Inlet compositions of the reacting mixture used for the present simulations are given in Table 4.

Table 4

The comparison between rapeseed oil methyl ester experimental data and computed results is shown in Figs. 8 and 9 and is globally satisfactory. The model allows matching the mole fraction profiles of most products of the reaction. At $\phi = 0.5$, mole fractions of 1-alkenes are well reproduced by the model except for ethylene and 1-hexene, whose mole fractions are slightly underpredicted. At $\phi = 1$, the ethylene mole fraction is still underpredicted whereas the mole fractions of 1-butene is too high, especially when the temperature increases. The same trend was also observed by Dagaut et al. using their n-cetane mechanism except for ethylene (slightly overpredicted in their simulations compared to experiments) [13]. The model predicts formation of hydrogen at temperatures somewhat lower than in the experiments.

At both equivalence ratios, CO and CO_2 mole fractions are slightly under predicted but their mole fraction profiles are much better than the mole fractions profiles obtained using the n-cetane mechanism. The early production of CO_2 occurring in the range of temperatures 800 - 850 K is much better reproduced by the methyl decanoate mechanism than by the n-cetane mechanism. Dagaut et al. recognized this shortcoming of using an n-hexadecane mechanism for RME simulations, and they discussed how the structure of the methyl esters in RME lead to early CO and CO_2 that cannot be captured in an n-alkane reaction mechanism. Routes of formation of these species are detailed later in the paper. Dagaut et al. also commented that the use of n-hexadecane produced mole fractions of large 1-olefins larger than they found in their RME experiments, which they attributed to the longer uninterrupted carbon chains in n-hexadecane than in the methyl ester fuels.

Figure 8

Figure 9

JSR simulations with a mixture of methyl decanoate and n-heptane. The methyl decanoate mechanism was modified slightly to run a mixture of methyl decanoate and n-heptane: unimolecular decomposition reactions and H atom abstractions of radicals from n-heptane added to take to account for the presence of this additional species in the inlet flow. Reactions of the resulting n-heptyl radicals were already included in the methyl decanoate mechanism. N-heptane was chosen as a co-reactant because it has been used frequently as a surrogate for diesel fuels and because it did not require the addition of too many reactions. An equimolar blend of methyl decanoate ($C_{11}H_{22}O_2$) and n-heptane (C_7H_{16}) enabled us to match the number of carbon and oxygen atoms in rapeseed oil methyl ester ($C_{17.92}H_{33}O_2$) used in the experiments [13]. It is worth noticing that the number of H atoms in the surrogate (38) is still higher than the number of H-atoms in rapeseed oil methyl esters. Inlet mole fractions have also been deduced from the values used by Dagaut et al. for their simulations. Inlet compositions used for the simulations are summarized in Table 5.

Table 5

Computed results from the methyl decanoate/n-heptane mechanism are very close to those obtained with the methyl decanoate model, and both simulations lead to similar reactivity. The CO_2 mole fraction is slightly lower in the case of the blend surrogate than in the case of the neat methyl decanoate surrogate. This is due to the fact that the inlet mole fraction of methyl decanoate (and therefore of the ester group) was higher in the case of the simulations run with neat methyl decanoate than in the case of the simulations performed with the blend surrogate. However, the predicted CO_2 levels from both surrogates containing methyl decanoate were considerably larger than those calculated from the n-hexadecane mechanism of Dagaut et al. [13].

Mole fractions of the 1-alkenes are higher in the case of the blend surrogate than for the neat surrogate, due to the presence of n-heptane as co-reactant and to the fact that β-scission decomposition products of alkyl and ester-alkyl radicals are not quite identical. Decomposition of alkyl radicals leads to 1-alkenes and smaller alkyl radicals which then decompose in turn, while decomposition of ester-alkyl radicals leads to the formation of 1-alkenes and smaller alkyl-ester radicals or unsaturated ester and alkyl radicals.

Figure 10

Figure 11

Formation of unsaturated methyl esters. In a recent paper, Dagaut and Gaïl reported the formation of methyl esters with a double bond at the extremity of the hydrocarbon chain (methyl-2-propenoate, methyl-3-butenoate, methyl-4-pentenoate and methyl-5-

hexenoate). Experiments have been performed in a jet stirred reactor, at a pressure of 10 atm, a residence time of 0.5 s and at an equivalence ratio of 1. The reactants were a mixture of Jet fuel (A1) and RME (80/20) in N_2/O_2.

The methyl decanoate model has not been compared to these results in a direct way because Jet-A1 is a blended fuel containing hundreds of different types of hydrocarbons. Dagaut and Gaïl used a three components surrogate (n-decane, n-propylbenzene, and n-propylcyclohexane) for the modeling of the oxidation of Jet-A1 [15].

Thus a qualitative comparison between the methyl decanoate model and these results has been performed. Both the experiments and model show that the bulk of the unsaturated methyl ester produced is methyl-2-propenoate. It is also observed that, at given experimental conditions, mole fractions of unsaturated esters decrease with number of carbons on their hydrocarbon chain. In other words, the mole fraction of methyl-2-propenoate is higher than the mole fraction of methyl-3-butenoate and so on. This is also the case with 1-olefins. Ethylene is more abundant than propene and so on. Mole fractions of unsaturated esters computed by the methyl decanoate model are in agreement with these experimental observations (Figure 12). Experimental and computed distributions of these four methyl esters have been compared. The distribution computed with our model is quite similar to the distribution obtained in Dagaut and Gaïl's experiments.

Figure 12

Route of formation of CO$_2$ at low temperature. The two models (neat methyl decanoate and methyl decanoate/n-heptane) make it possible to reproduce the early formation of CO_2 observed in the experiments by Dagaut et al.. A rate of production analysis was

performed for the simulation at $\phi = 0.5$, T = 800K, P = 10 atm and $\tau = 1$ s with the methyl decanoate mechanism to highlight the route of production of CO_2 at low temperature.

At these conditions, CO_2 is formed through four elementary reactions: the decomposition of the radical OCHO (+M) to H + CO_2 (+M) (38%), the decomposition of HOCHO to H_2 + CO_2 (31%), the reaction of OH + CO leading to H + CO_2 (17%), and the decomposition of the radical CH_3OCO to CH_3+ CO_2 (7%). With the exception of the reaction of CO with OH and the decomposition of HOCHO to H_2 + CO_2, the other two reactions derive uniquely from the methyl ester group in methyl decanoate and would not occur in the oxidation of n-hexadecane or any other n-alkane fuel.

The radical OCHO derives primarily from the decomposition of radicals involved in the low temperature part of the mechanism (Table 6). These radicals have a carbonyl group on the ester methyl group and a radical center on the carbon atom in the β position of the ester carbonyl group. They come from the decomposition of ester cyclic ethers formed in the low temperature part of the mechanism. Figure 13 displays the complete sequence of reactions from an alkyl-ester radical to CO_2 via the radical OCHO. It is interesting to see that one oxygen atom in this molecule of CO_2 comes from the non carbonyl part of the ester group and the other oxygen atom from the oxygen molecule involved in the reaction of addition. This let us think that this sequence of reactions is likely also valid for fuels with an embedded oxygen atom like ethers. The radical HOCHO mainly comes from the reaction of addition of the OH radical to formaldehyde. The radical CH_3OCO mainly comes from the decomposition of the numerous radicals having a radical center on the carbon atom in the γ position of the ester carbonyl group (Figure 14).

Table 6

Figure 13

Figure 14

According to the rate of production analysis performed with the blend surrogate, the CO_2 production occurs via the same four main routes. The rates of these reactions are very similar except for the reactions involving indirectly the ester group of methyl decanoate: the decomposition of the radicals OCHO and CH_3OCO (Table 7). Rates of these reactions are lower in the case of the blend surrogate because the inlet mole fraction of methyl decanoate is less than in the case of the neat surrogate.

Table 7

These results are also consistent with the rate of production analysis we performed in similar conditions with the methyl butanoate mechanism developed by Fisher et al. [8]. For methyl butanoate, the main source of CO_2 is the decomposition of the cyclic ether formed in the low temperature part of the mechanism via OCHO (38%). The second source of formation of CO_2 is not the decomposition of HOCHO, but the decomposition of the radical CH_3OCO (24%). This difference can be explained by the fact that the kinetic parameters of the two reactions of decomposition of this radical

($CH_3OCO = CH_3 + CO_2$ and $CH_3OCO = CH_3O + CO$) have been updated in the methyl decanoate mechanism from a recent work of Glaude et al. about dimethyl carbonate [36].

Early CO_2 production from the methyl ester group in methyl decanoate has important practical implications in diesel ignition and soot production. Recent kinetic modeling of ignition under diesel engine conditions [4,37] showed how the presence of oxygen atoms in the fuel can reduce soot production from the fuel molecule. However, if that oxygen immediately produces CO_2, as in methyl butanoate and methyl decanoate (and, by implication, in all biodiesel fuels), that fuel-bound oxygen is less effective in reducing soot production.

Reaction path analysis. A flow rate analysis of the model has been performed at $\tau = 1$ s, at P = 10 atm, $\phi = 0.5$ and at two different temperatures (800 and 1040 K) in order to cover the low and high temperature regions.

At low temperature (800 K), the reactant (methyl decanoate) is mainly consumed by the reactions of H-atom abstractions with hydroxyl radicals (95.3% in the conditions of the kinetic analysis). Mainly secondary alkylic and secondary allylic radicals are formed through these reactions. Fates of these radicals are very similar so we can focus on one of them to continue the reaction path analysis. Let's choose md3j (Figure 15). This radical mainly reacts through two types of reactions: addition to O_2 (63%) to form a peroxy radical (md3o2) and isomerizations through cyclic transition state (28%) forming two other radicals (md7j, 21% and mdmj, 7%) with very similar structures (they can react the same manner as md3j). It is worth noting that both radicals are formed through six member ring isomerizations which have the lowest activation energy (isomerizations

through smaller rings are more difficult at low temperature). In this temperature region, reactions of β-scission don't take place because of their higher activation energy. Let's consider now the fate of the peroxy radical md3o2. It entirely reacts by isomerizations through cyclic transition state (5, 6 and 7 member rings). The easiest isomerization is the one going through a six member cyclic transition state leading to the hydroperoxy radical called md3ooh5j in the mechanism: 52% (Figure 16). The seven member isomerization leading to md3ooh6j represents 27% of the consumption of md3o2 and the two five member isomerizations forming md3ooh2j and md3ooh4j 13% and 8% respectively. md3ooh4j (and so md3ooh2j) can react through the three types of reaction presented in Figure 6: second addition to O_2 (57%), C-O β-scission forming an unsaturated methyl esters and HO_2 (22%), decomposition to a cyclic ether + OH (21%). md3ooh5j cannot react by C-O β-scission. It reacts by concerted elimination through a six member ring (53%) forming an olefin, an aldehyde and OH, second addition to O_2 (27%) and decomposition to a cyclic ether plus OH (20%). md3ooh6j reacts only through the second addition to O_2 and the decomposition to a cyclic ether and OH. O_2QOOH radicals from the second additions to O_2 decompose to ketohydroperoxide and OH as shown on Figure 7. The ketohydroperoxide then decomposes to a radical and a second OH providing chain branching.

Figure 15

Figure 16

At higher temperature (1040 K), the conversion of the reactant is almost 100% at the conditions of the kinetic analysis. The reactant is mainly consumed by reactions of unimolecular initiation (presented in Table 2) forming free radicals (Figure 17). In this

25

temperature region, the radicals from the initiations mainly react through two kinds of reactions: β-scissions and isomerizations. As an example, the 1-octyl radical (C_8H_{17}) leads to ethylene plus 1-hexene by β-scission (7%) and to the 4-octyl radical by isomerizations through 5 and 6 member rings (24 and 68% respectively). It is worth noting that in this temperature region the reaction of addition to O_2 doesn't take place because the reverse dissociation reaction becomes much more important. Unsaturated species (olefins and unsaturated esters) obtained by β-scission decompositions of the radicals can react by unimolecular initiations (by breaking of the C-C and C-H allylic bonds) and by retroene reactions (Figure 18).

Figure 17

Figure 18

The kinetic analysis shows that some reactions play a major role in the oxidation of methyl decanoate. Some of these reactions have been the subject of several studies and the associated kinetic parameters are relatively well known. This is mainly the case for the reactions which intervene at high temperature: unimolecular initiations, β-scission decompositions, isomerizations, retroene reactions and H-atom abstractions with small radicals. Reactions involved in the low temperature region have more uncertainties: this is the case for the reactions of isomerization of peroxy radicals (RO_2) to hydroperoxy radicals (QOOH). Rate constants for these reactions are from Curran et al. [21] This treatment does not take into account direct eliminations from RO_2 (leading to olefins + HO_2) which intervenes in the more recent scheme proposed for the low temperature of alkyl radicals [28-30]. Isomerizations of RO_2 to QOOH through cyclic transition states involving the ester function are very uncertain (as shown in Figure 13). Quantum

calculations would be useful to acquire new data. Isomerization and decomposition of hydroperoxy peroxy radicals to ketohydroperoxide and OH may have uncertainties too. Also, there is a lack of data concerning the decomposition of hydroperoxy radicals to cyclic ethers plus OH and the reactions of the cyclic ethers. These reactions need further investigation.

Methyl decanoate ignition delay times comparison with n-decane and n-heptane

In the previous section, we have examined the differences between the use of kinetic mechanisms for n-alkane and methyl ester fuels to simulate experimental results for combustion of methyl ester fuels. In this section, we address the reverse problem, the use of a kinetic mechanism for a methyl ester to simulate experimental results for combustion of an n-alkane fuel. The overall goal of this work is to compare how closely the combustion properties of large n-alkane fuels and related large methyl esters resemble each other, and how well their kinetic reaction mechanisms can reproduce the combustion properties of each other.

Ignition delay times calculated from the methyl decanoate mechanism were compared to experimental results for n-decane. N-decane was selected for the comparison because it has the same number of carbon atoms as the alkyl chain of methyl decanoate, and numerous experimental data of the oxidation of n-decane are available.

Davidson et al. [19] measured OH mole fraction/time histories behind reflected shocks in n-decane ignition. Experiments performed at a fuel mole fraction of 300 ppm, at temperatures ranging from 1479 to 1706 K, at pressures from 2.08 to 2.21 atm, and at an equivalence ratio of 1.0 (99.505 % Argon) have been compared to simulations from

the methyl decanoate mechanism (simulations were performed with an average pressure of 2.15 atm). The agreement between the two sets of data is quite good in these conditions (Figure 19). Calculated OH mole fraction time histories for three temperatures are shown in Figure 20 (actual pressures were used for the simulations). These three profiles are very close to the experimental ones obtained by Davidson et al. for n-decane [19] except for the experiment at 1525 K, where the computed results are very similar to the measurements but delayed compared to the experimental results. The methyl decanoate mechanism reproduces the two stage ignition observed during the n-decane experiments: a first, very early and rapid increase of the OH mole fraction (with a small overshoot visible at the lowest temperatures), then an induction period which is more or less well defined according to the temperature, and a second rapid increase of the OH mole fraction to a level that is very well reproduced by the kinetic mechanism.

Figure 19

Figure 20

Simulations performed with the methyl decanoate mechanism were also compared to shock tube experiments for n-decane/air mixtures performed by Pfahl et al. [38] over a broader range of temperatures covering both the high and low temperature regions. Experimental conditions of these measurements were 700 – 1300 K, 12 – 50 atm, equivalence ratio of 1 (in air). These experimental conditions are particularly relevant to conditions in internal combustion engines. Figure 21 displays a comparison of

experimental ignition delay times for n-decane and calculated ones from the methyl decanoate mechanism with constant volume combustion behind the reflected shock wave assumed. At the highest temperatures (more than 800 K at 12 atm and more than 1000 K at 50 atm) experimental and calculated data are in a relatively good agreement. At the lowest temperatures, below the negative temperature coefficient region, the methyl decanoate mechanism leads to ignition delay times slightly longer than experimental ones for n-decane. This trend was also observed in the case of the modeling of n-heptane. It is likely due to uncertainties in kinetic parameters used in the mechanism (reaction of decomposition of hydroperoxy compounds involved in the low temperature part of the mechanism).

Figure 21

The molecular structure of methyl decanoate can be visualized as very similar to n-decane; both have the same chain of 10 C atoms, populated by a lot of secondary C-H bonds. This mechanism, and prior mechanisms for n-alkanes in general and n-heptane in particular, show how the negative temperature coefficient (NTC) region is caused by the temperature dependence of the alkylperoxy radical isomerization reaction pathways. This NTC feature has been seen here for the combustion of methyl decanoate. In comparing methyl decanoate and n-decane, however, it is evident that the presence of the methyl ester group at one end of the carbon atom chain tends to reduce the number of RO_2 isomerization reactions that can occur in this NTC region. When the straight-chain is as long as 10 C atoms, elimination of a few RO_2 and O_2QOOH isomerization pathways

due to the presence of the methyl ester group does not produce a significant reduction in the rate of low temperature chain branching, but it is a reduction large enough to be observed as seen in Figure 21. This has important implications with respect to development of surrogate fuels and mechanisms for practical hydrocarbon fuels. As already observed earlier, the n-alkane mechanism cannot reproduce the early CO_2 production of the methyl ester fuels, but these calculations indicate that the methyl ester mechanism can reproduce the heat release and ignition delay of the corresponding n-alkane fuel very well.

Comparison with engine experiments

In the next series of calculations, predictions using the chemical kinetic model were compared to experiments performed in a motored engine. The experiments were performed by Szybist et al. using premixed charges of fuel and air in a CFR engine with adjustable compression ratio [17,18]. Fuels used in this study were n-heptane, commercial diesel fuel and methyl decanoate. Exhaust analysis was performed with a FTIR spectrometer. Quantified compounds were carbon monoxide, carbon dioxide, formaldehyde, and acetaldehyde. In the case of methyl decanoate, condensable compounds in the exhaust gas, which were trapped before the FTIR analysis, were analyzed with a GC/MS system, allowing identification of many products of the reaction but not their quantification. Pressure measurements in the cylinder were performed through a piezoelectric pressure transducer.

Simulations have been performed for both n-heptane (with the mechanism developed by Curran et al. [20]) and methyl decanoate with the "Internal Combustion

Engine" model (single zone) of the software Chemkin 3. Characteristics of the engine required for the simulations are the displaced volume (612 cm^3), the engine speed (900 rpm), and the ratio of the length of the engine connecting rod to the crank radius (4.5). Intake valve closure (IVC) was 24 degrees after dead bottom center which corresponds to a starting crank angle of 214 degrees in the "Internal Combustion Engine" model. The starting pressure used for the simulations was the measured pressure at IVC (1.05 atm). Very little information about the starting temperature and the heat losses was available, making simulations difficult and requiring some assumptions. Intake charge temperature was 383.15 K in the case of n-heptane and 503.15 K in the case of methyl decanoate (boiling point: 497 K at 1 atm) whereas the wall of the cylinder was cooled with water at 373.15 K. So for the simulations with n-heptane, the starting temperature was chosen equal to 383.15 K. In the case of methyl decanoate, the intake charge temperature was much higher than the cylinder wall temperature and the charge was likely cooled during the intake. We chose 423.15 K as starting temperature so that the calculated critical compression ratio matches the experimental one. The critical compression ratio is the minimum compression ratio at which autoignition occurs. No heat losses were considered in the calculations because they were not quantified and simulations have been performed with the lowest experimental equivalence ratio (0.25) in order to have the least heat release and minimizing heat transfer from the gas to the wall of the cylinder.

The residual gases remaining in the combustion chamber after the end of a cycle influence the reactivity of the next cycle. To account for the effect of residual gases, the gases remaining at the end of the expansion stroke of the first computed cycle were used to specify the composition and the temperature of the residual gases for the next

computed cycle. At the start of the next cycle, the fraction of residual gases to total charge was assumed to be the inverse of the compression ratio. In this manner, consecutive cycles were performed until the steady state was reached [39].

Figure 22

Motored Engine simulations with n-heptane. We first compared model predictions to the experiments for n-heptane because the n-heptane mechanism is more mature and well-validated than the methyl decanoate mechanism. If the comparison is successful, it can give confidence that the modeling approach used is valid. Simulations were performed by varying the compression ratio over the range of experimental investigation (4.5 to 9.5). The fresh charge was composed of n-heptane in air with an equivalence ratio of 0.25. Table 8 displays the calculated mass fractions (% fuel C) of CO, CO_2, CH_2O and CH_3CHO at the end of the expansion stroke for six consecutive cycles at a compression ratio of 6, where the 1st cycle starts with 100% fresh charge. The evolution in the mass fractions from cycle 1 to cycle 6 shows that the remaining gases in the cylinder have an influence on the kinetics of the reaction, for this compression ratio where ignition does not occur.

Table 8

Figure 23 shows the comparison between the computed mass fractions at the end of the expansion stroke to those measured in the exhaust of the motored engine fueled by

n-heptane. The agreement between calculated and experimental data [18] is globally satisfactory. The calculated ignition occurs at about the same compression ratio as in the experiments (slightly below CR=8). This shows that the overall reactivity of the n-heptane model is about right. The simulated ignition is rather sharp whereas the experimental one is much less abrupt. This can be explained by the fact that the "Internal Combustion Engine" model used for the simulation is a single zone model (concentrations are assumed to be homogeneous inside the cylinder) which is not the case in the real engine used for the experiments. CO and CO_2 mole fraction profiles are rather well reproduced by the model, with very low levels of CO_2 prior to ignition. Before the ignition occurs the model under-predicts the mole fraction of acetaldehyde by a factor of 1.3 and over-predicts that of formaldehyde by a factor of 2. These levels of precision are quite good for engine data analyses and illustrate the challenges of comparing single-zone simulations with real engine experiments.

Figure 23

Motored engine simulations with methyl decanoate. Based on the positive results for n-heptane, simulations were performed with the methyl decanoate mechanism and compared to experimental measurements over the range of compression ratios 4.4 to 5.6. The fresh charge was composed of methyl decanoate in air with an equivalence ratio of 0.25. These calculations were very time consuming compared to the simulations with n-heptane because of the size of the mechanism (about 3 hours CPU time for one cycle on a 4 GHz Intel Pentium™ 4 processor PC, compared with 10 CPU minutes for n-heptane).

With the added need to compute at least 6 cycles to achieve steady state, these calculations become very ambitious and resource intensive. One set of comparison curves represents about over 50 computed cycles and 160 hours of CPU time. The comparison between the computed and experimental results is shown in Figure 24. The starting temperature has been adjusted so that the computed critical compression ratio is very close to the experimental one. The computed critical compression ratio is sensitive to the charge temperature assumed at intake value closing (423 K). This temperature is a reasonable value lying between the limiting temperatures of the wall (373 K) and the intake (503 K). If the chemical kinetic model was too reactive or too unreactive, the needed temperature at intake valve closing would have been outside these experimental temperature limits. The agreement between computed and experimental mass fractions is again globally satisfactory. With methyl decanoate as a fuel, the model predicts a mole fraction of formaldehyde higher than that of acetaldehyde, in agreement with the experiments. The mole fraction of carbon dioxide is well reproduced and is much higher than in the n-heptane case, as shown both in the experimental measurements and in the model predictions for methyl decanoate. This is due to the additional formation paths for carbon dioxide from the ester chemistry present in methyl decanoate combustion. On the other hand, the mole fraction of carbon monoxide is over predicted. As the compression ratio increases, mass fractions of CO and CO_2 go up whereas mass fractions of acetaldehyde and formaldehyde go down. These trends and the high mole fraction of CO are due to overpredictions of the temperature. For example, at CR=4.8 the temperature at the top dead center reaches 889 K, which is likely too high because heat losses were not taken into account in these simulations. This elevated temperature is confirmed by an

elevated pressure at the end of compression (the calculated pressure is about 1 bar higher than the experimental value). However, if heat losses are included, it is likely that the computed critical compression ratio of methyl decanoate would be too low. At this point, we thought we had gained about as much information as we could derive from these comparisons, given all the uncertainties in modeling these experiments (e.g. nonhomogeneities in the chamber) and the large computing and manpower resources required. Overall, the most significant result of these simulations is the kinetic explanation of the elevated CO_2 levels at low compression ratios that were observed in the experiments for methyl decanoate, which translates into early CO_2 production in actual engine cycles, a feature which makes biodiesel fuels different from conventional diesel fuels.

Figure 24

Comparison with condensable compounds in the exhaust. Szybist et al. performed a qualitative analysis of the exhaust condensates from the engine by GC/MS. The species which were identified during this study were mainly methyl esters, methyl esters with a ketone group, and carboxylic acids. Other species like ketones and aldehydes were also observed.

In the range of temperatures corresponding to the region where compression ratios do not lead to ignition (below 900 K), the methyl decanoate mechanism predicts the formation of numerous methyl esters with one double bond (either at the extremity of the alkyl chain or conjugated with the double C=O bond of the ester group) as well as

1-alkenes. 1-alkenes and methyl esters with the double bond at the terminal position mainly come from the decomposition by C-C bond β-scission of alkyl and alkyl-ester radicals. Methyl esters with the double bond at the conjugated position are obtained from the decomposition by C-H bond β-scission of 3-alkyl-ester radicals (Figure 25).

Figure 25

The model also predicts the formation of aldehydes and methyl esters with a carbonyl group at the extremity of the alkyl chain. These species are obtained by decomposition by C-C bond β-scission of alkoxy and alkoxy-ester radicals. These last radicals are formed by addition of OH radicals to the double bond of alkenes and unsaturated esters followed by internal isomerizations involving the H-atom of the hydroxyl group. Organic acids are generated from the recombination of H-atoms and carboxylate radicals. Carboxylate radicals are derived from decomposition of some hydroperoxides (Figure 26).

Figure 26

The model also predicts the formation of hetero-cyclic species like cyclic ethers, but not 2-(3H)-furanone-5-ethyldihydro and 5-methoxycarbonylpentan-4-olide which were identified by GC/MS.

Conclusions

In this study, a detailed chemical kinetic oxidation mechanism for methyl decanoate, a surrogate for biodiesel fuel, has been developed by following the rules previously used for modeling n-heptane oxidation. Experimental data for the validation were very scarce and some of them have been performed in non ideal conditions that are difficult to model. The model was compared to rapeseed oil methyl ester experiments in a jet stirred reactor. This model (and the blend surrogate model including n-heptane chemistry) reproduced the overall reactivity as well as the mole fractions of the products of the reaction. An important feature of this mechanism is its ability to predict the early formation of carbon monoxide and carbon dioxide. The kinetic analysis of the model showed that early formation of these two species is linked to the presence of the ester group in the methyl decanoate molecule.

The methyl decanoate model was also compared with n-decane experimental results from shock tube experiments. Calculated ignition delay times and OH profiles were in very good agreement with n-decane experiments, showing that the reactivity of large methyl esters is very similar to the reactivity of n-alkanes of similar size. This mechanism was compared with methyl decanoate oxidation experiments in a motored engine. Although these experiments were not well characterized and the numerical model used for the computations was too simplified, the agreement between calculated and experimental mole fractions was qualitatively satisfactory.

Further refinements are possible to improve capabilities for biodiesel simulations. Real biodiesel fuels are mixtures of several esters, some of them having one, two or three

double bonds in their alkyl chains, as shown above in Fig. 1. We intend to develop additional submodels, based on methyl decanoate, to highlight the influences of the presence of double bonds in the alkyl chain and provide very realistic surrogate fuel mechanisms for real biodiesel fuels from various origins and having different compositions.

Overall, it appears that both n-hexadecane and methyl decanoate are acceptable surrogates for biodiesel fuel, based on the comparisons with the work of Dagaut et al. [13] and the present work. One strength of the present mechanism is its ability to reproduce the effects of the methyl ester group in all of the major components of soybean and rapeseed methyl esters. The n-hexadecane mechanism of Dagaut et al. predicts mole fractions of large olefin species that are larger than those measured in rapeseed methyl ester fuel combustion, but the present methyl decanoate mechanism does not include olefins larger than C_{10} and cannot predict mole fractions of any species larger than that. The present methyl decanoate mechanism is also unique by including low temperature reaction pathways that enable it to address such important practical problems as diesel ignition and sooting, as well as combustion in HCCI engines, all of which require a kinetic description of the low temperature kinetics of the fuel. Since the boiling point of methyl decanoate is 497 K, future experimental data in heated shocktubes and rapid compression machines may be acquired and used to further test this chemical kinetic mechanism. This is not the case for even higher molecular weight methyl esters whose high boiling points make acquisition of experimental data in these devices very difficult and limit the validation of their associated chemical kinetic mechanisms. Thus, methyl decanoate is a convenient test fuel for detailed chemical kinetic mechanisms of biodiesel

surrogates. Ultimately, a full, detailed, high and low temperature mechanism for the C_{16} and C_{18} saturated and unsaturated species that are in real biodiesel fuels will be required. One additional accomplishment of the present mechanism development for methyl decanoate is a demonstration that such a biodiesel kinetic mechanism is already feasible and accessible by extending this mechanism to include a longer alkane chain.

Acknowledgment

Supporting information

Thermodynamic database

Chemical kinetic model

References

1. A. Tsolakis, A. Megaritis, M. L. Wyszynski, K. Theinnoi, Energ. 32 (2007) 2072-2080.

2. M. E. Tat, P.S. Wang, J. H. Van Gerpen, T. E. Clemente, J. Am. Oil Chem. Soc. 84 (2007) 865-869.

3. R.L. McCormick, J.D. Ross, M.S. Graboski, Environ. Sci. Technol. 21 (4) (1997) 1144-1150.

4. C.K. Westbrook, W.J. Pitz, H.J. Curran, J. Phys. Chem. A (110) (2006) 6912-6922.

5. J. Van Gerpen, B. Shanks, R. Pruszko, D. Clements, G. Knothe, Biodiesel Production Technology, National Renewable Energy Laboratory subcontractor report NREL/SR-510-36244, 2004.

6. B. Freedman, M.O. Bagby, J. Am. Oil Chem. Soc. 67 (1990) 565-571.

7. W.E. Klopfenstein, J. Am. Oil Chem. Soc. 62 (1985) 1029-1031.

8. E.M. Fisher, W.J. Pitz, H.J. Curran, C.K. Westbrook, Proc. Combust. Inst. 28 (2000) 1579-1586.

9. W.K. Metcalfe, S. Dooley, H.J. Curran, J.M. Simmie, A.M. El-Nahas, M.V. Navarro, J. Phys. Chem. 111 (19) (2007) 4001-4014.

10. S. Gaïl, M.J. Thomson, S.M. Sarathy, S.A. Syed, P. Dagaut, P. Diévart, A.J. Marchese, F.L. Dryer, Proc. Combust. Inst. 31 (1) (2007) 305-311.

11. S.M. Sarathy, S. Gaïl, S.A. Syed, M.J. Thomson, P. Dagaut, Proc. Combust. Inst. 31 (1) (2007) 1015-1022.

12. T. Vaughn, M. Hammill, M. Harris, A.J. Marchese, Ignition Delay of Bio-Ester Fuel Droplets, SAE Technical Paper Series, 2006-01-3302.

13. P. Dagaut, S. Gaïl, M. Sahasrabudhe, Proc. Combust. Inst. 31 (2) (2007) 2955-2961.

14. A. Ristori, P. Dagaut, M. Cathonnet, Combust. Flame 125 (3) (2001) 1128-1137.

15. P. Dagaut and S. Gaïl, J. Phys. Chem. A 111 (2007) 3992-4000.

16. J. R. Pedersen, Å. Ingemarsson, J. O. Olsson, Chemosphere 38 (11) (1999) 2467-2474.

17. J.P. Szybist, J. Song, M. Alam and A.L. Boehman, Fuel Process. Technol. 88 (7) (2007) 679-691.

18. J.P. Szybist, A.L. Boehman, D.C. Haworth, and H. Koga, Combust. Flame 149 (1-2) (2007) 112-128.

19. D.F. Davidson, J.T. Herbon, D.C. Horning DC, R.K. Hanson, Int. J. Chem. Kinet. 33 (12) (2001) 775-783.

20. H.J. Curran, P. Gaffuri, W.J. Pitz, C.K. Westbrook, Combust. Flame 129 (2002) 253-280.

21. H.J. Curran, P. Gaffuri, W.J. Pitz, C.K. Westbrook, Combust. Flame 114 (1998) 149-177.

22. H.J. Curran, Int. J. Chem. Kinet. 38 (4) (2006) 250-275.

23. D.J. Henry, M.L. Coote, R. Gomez-Balderas, L. Radom, J. Am. Chem. Soc. 126 (6) (2004) 1732-1740.

24. D.M. Matheu, W.H. Green, J.M. Grenda, Int. J. Chem. Kinet. 35 (3) (2003) 95-119.

25. V. Warth, F. Battin-Leclerc, R. Fournet, P.A. Glaude, G.M. Come, G. Scacchi, Comput. Chem. 24 (5) (2000) 541-560.

26. K.D. King, Int. J. Chem. Kinet. 11 (1979), 1071-1080.

27. R.S. Zhu, J. Park, M.C. Lin, Chem. Phys. Lett. 408 (2005) 25-30.

28. H. Sun, Joseph W. Bozzelli, J. Phys. Chem. A 108 (10) (2004) 1694-1711.

29. C.Y. Sheng, J.W. Bozzelli, A.M. Dean, A.Y. Chang, J. Phys. Chem. A 106 (2002) 7276-7293.

30. J.D. DeSain, S.J. Klippenstein, J.A. Miller, C.A. Taatjes, J. Phys. Chem. A 107 (2003) 4415-4427.

31. E.J. Silke, W.J. Pitz, C.K. Westbrook, M. Ribaucour, J. Phys. Chem. A. 111 (19) (2007) 3761-3775.

32. K.A. Sahetchian, R. Rigny, J. Tardieu De Maleyssie, L. Batt, M. Anwar Khan, S. Mathews, Proc. Combust. Inst. 24 (1992) 637-643.

33. E.R. Ritter, J. W. Bozzelli, Int. J. Chem. Kinet. 23 (1991) 767-778.

34. S.W. Benson, Thermochemical Kinetics, John Wiley and Sons Inc., New York, 1976.

35. A.M. El-Nahas, M.V. Navarro, J.M. Simmie, J.W. Bozzelli, H.J. Curran, S. Dooley, W. Metcalfe, J. Phys. Chem. A 111 (19) (2007) 3727-3739.

36. P.A. Glaude, W.J. Pitz, M.J. Thomson, Proc. Combust. Inst. 30 (2005) 1111-1118.

37. C. J. Mueller, W. J. Pitz, L. M. Pickett, G. C. Martin, D. L. Siebers and C. K. Westbrook, Effects of Oxygenates on Soot Processes in DI Diesel Engines: Experiments and Numerical Simulations, SAE 2003-01-1791, 2003 Arch T. Colwell Merit Award Paper, 2003.

38. U. Pfahl, K. Fieweger, G. Adomeit, Proc. Combust. Inst. (1996) 781-789.

39. H.J. Curran, P. Gaffuri, W.J. Pitz, C.K. Westbrook, W.R. Leppard, Autoignition Chemistry of the Hexane Isomers: An Experimental and Kinetic Modeling Study, SAE Technical Paper Series 952406, 1995.

Esters	Soybean biodiesel	Rapeseed biodiesel
methyl palmitate	6-10%	4.3%
methyl stearate	2-5%	1.3%
methyl oleate	20-30%	59.9%
methyl linoleate	50-60%	21.1%
methyl linolenate	5-11%	13.2%

Table 1: Average compositions (%) of soybean and rapeseed biodiesels [5].
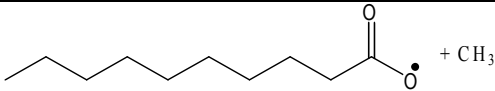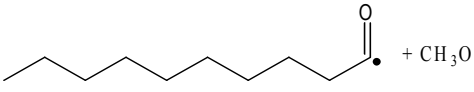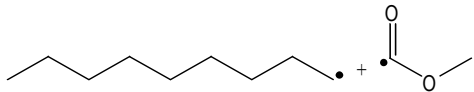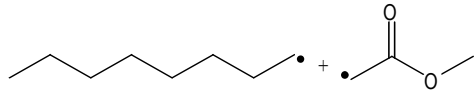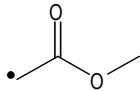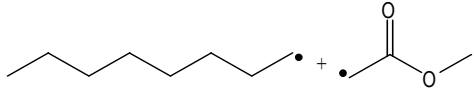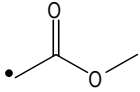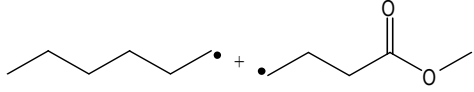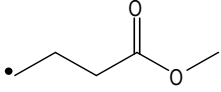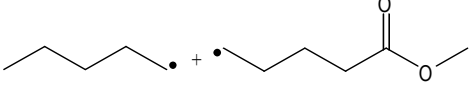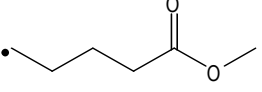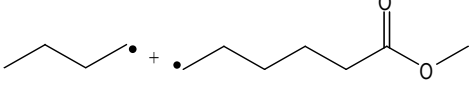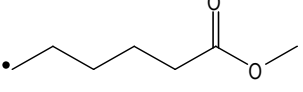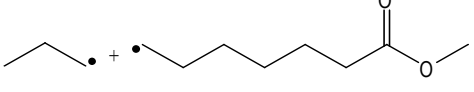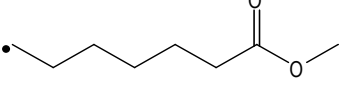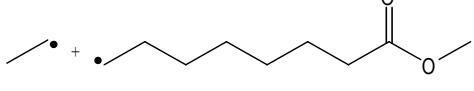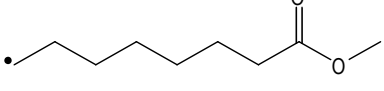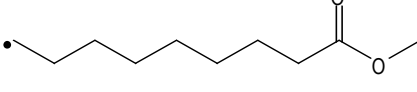
Reaction of recombination	Rate constant ($cm^3.mol^{-1}.s^{-1}$)
+ CH_3	3.0×10^{13}
+ CH_3O	3.0×10^{13}
	1.8×10^{13}
	8.0×10^{12}
	8.0×10^{12}
	8.0×10^{12}
	8.0×10^{12}
	8.0×10^{12}
	8.0×10^{12}
	8.0×10^{12}
CH_3 +	3.0×10^{13}

Table 2: Reactions of recombination involving C-O and C-C bonds in methyl decanoate.

Reactions			A	b	Ea
R + O$_2$ = RO$_2$		R is a primary radical	4.52×10^{12}	0.0	0.0
		R is a secondary radical	7.54×10^{12}	0.0	0.0
		R is a tertiary radical	1.41×10^{13}	0.0	0.0
RO$_2$ = QOOH	5 atoms ring	primary H shifted	1.0×10^{11}	0.0	29.4
		secondary H shifted	1.0×10^{11}	0.0	26.85
		tertiary H shifted	1.0×10^{11}	0.0	24.1
	6 atoms ring	primary H shifted	1.25×10^{10}	0.0	24.4
		secondary H shifted	1.25×10^{10}	0.0	20.85
		tertiary H shifted	1.25×10^{10}	0.0	19.1
	7 atoms ring	primary H shifted	1.56×10^{9}	0.0	22.35
		secondary H shifted	1.56×10^{9}	0.0	19.05
		tertiary H shifted	1.56×10^{9}	0.0	17.05
	8 atoms ring	primary H shifted	1.95×10^{8}	0.0	25.55
		secondary H shifted	1.95×10^{8}	0.0	22.05
		tertiary H shifted	1.95×10^{8}	0.0	20.05
HO$_2$ addition to C=C bonds		to a primary carbon atom	1.0×10^{11}	0.0	10.75
		to a secondary carbon atom	1.0×10^{11}	0.0	11.75
QOOH = OH + cyclic ether		oxirane	6.0×10^{11}	0.0	22.0
		oxetane	7.5×10^{10}	0.0	15.25
		oxalane	9.37×10^{9}	0.0	7.0
		oxane	1.17×10^{9}	0.0	1.8

Table 3: Rate constants of the main reactions involving RO$_2$ and QOOH radicals

($k=A\times T^{b}\times exp(Ea/RT)$, Units: kcal, cm^3, mol, s).

Experimental conditions	P = 10 atm, ϕ = 0.5, τ = 1 s	P = 10 atm, ϕ = 1, τ = 1 s
Methyl decanoate	$8.18.10^{-4}$	$8.18.10^{-4}$
Oxygen	$2.44.10^{-2}$	$1.18.10^{-2}$
Nitrogen	$9.75.10^{-1}$	$9.87.10^{-1}$

Table 4: Inlet compositions of reacting mixtures used for methyl decanoate simulations in

the jet stirred reactor.

Experimental conditions	P = 10 atm, ϕ = 0.5, τ = 1 s	P = 10 atm, ϕ = 1, τ = 1 s
Methyl decanoate	5.10^{-4}	5.10^{-4}
n-Heptane	5.10^{-4}	5.10^{-4}
Oxygen	$2.47.10^{-2}$	$1.21.10^{-2}$
Nitrogen	$9.74.10^{-1}$	$9.87.10^{-1}$

Table 5: Inlet compositions of the reacting mixture used for the methyl decanoate - n

heptane surrogate simulations in the jet stirred reactor.
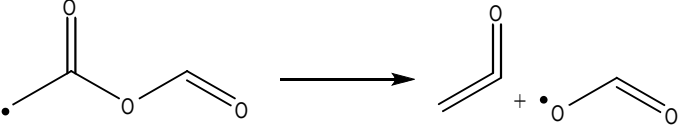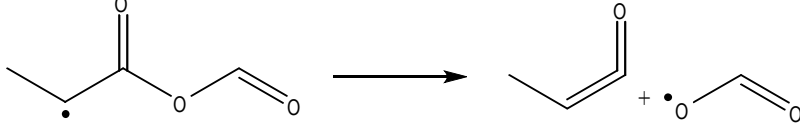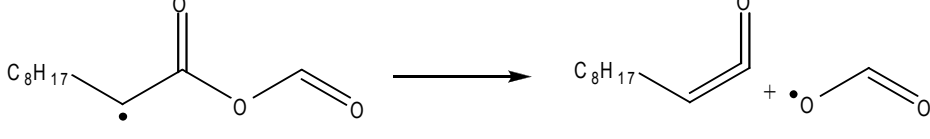
Reaction	Normalized Rate of Production (%)
	68
	4
	22

Table 6: Reactions leading to the formation of the radical OCHO.

Reactions	Rate of Production ($\times 10^8$, mol.cm^{-3}.s^{-1})	
	Blend Surrogate	Neat Surrogate
OCHO (+M) = H + CO_2 (+M)	1.54	2.43
HOCHO = H_2 + CO_2	2.20	2.03
OH + CO = H + CO_2	0.94	0.90
CH_3OCO = CH_3+ CO_2	0.41	0.61

Table 7: Rates of the main reactions leading to the formation of CO_2 (ϕ = 0.5, T = 800 K,

P = 10 atm and τ = 1 s).

Cycle	CO	CO_2	CH_2O	CH_3CHO
1	19.53	1.54	7.54	6.86
2	17.55	1.22	6.17	5.18
3	15.61	1.04	6.01	5.05
4	15.58	1.03	6.07	5.10
5	15.57	1.02	6.07	5.10
6	15.57	1.02	6.07	5.10

Table 8: Calculated mass fractions (% of fuel C) for six consecutive cycles at CR=6.
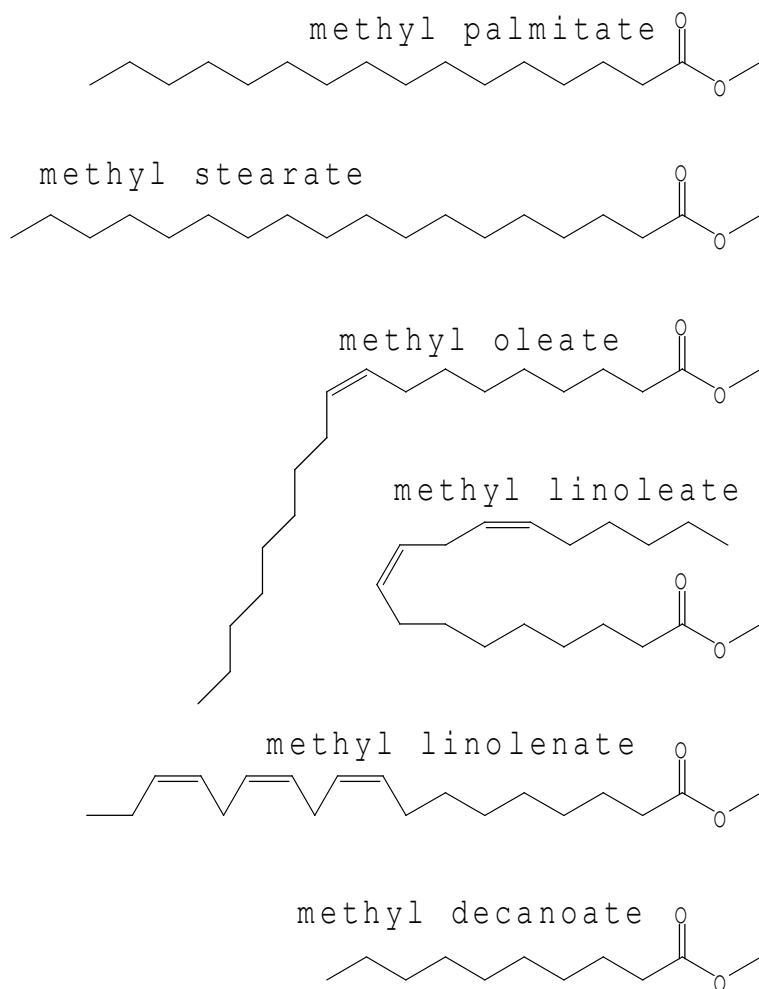
Figure captions:

Figure 1: Structure of the main components found in soybean and rapeseed oils methyl esters and of methyl decanoate.
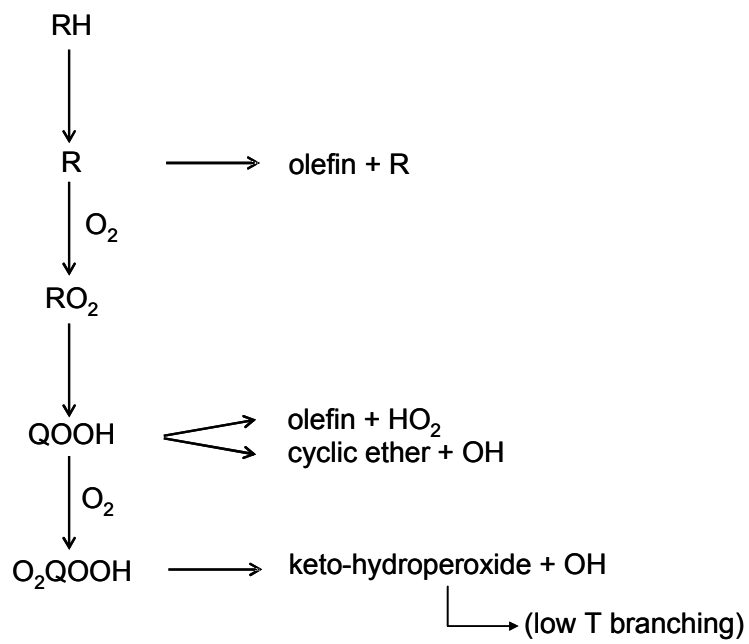
Figure 2: Primary oxidation reactions taken into account for the development of the methyl decanoate mechanism.
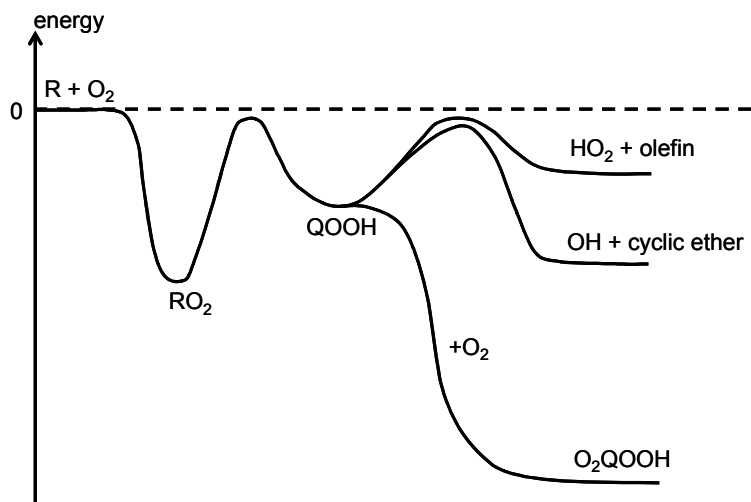
Figure 3: Potential energy diagram for the addition of R to O_2 and subsequent reactions (low temperature scheme used in the methyl decanoate mechanism).
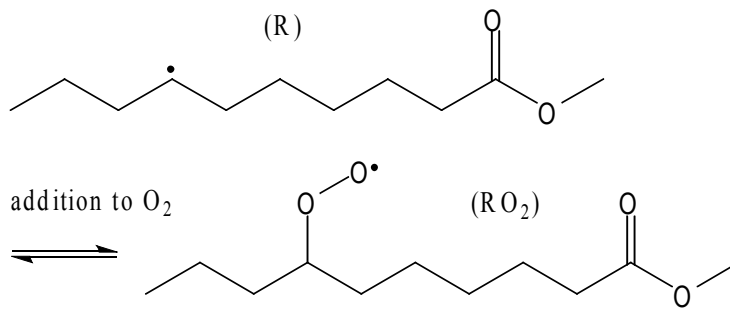
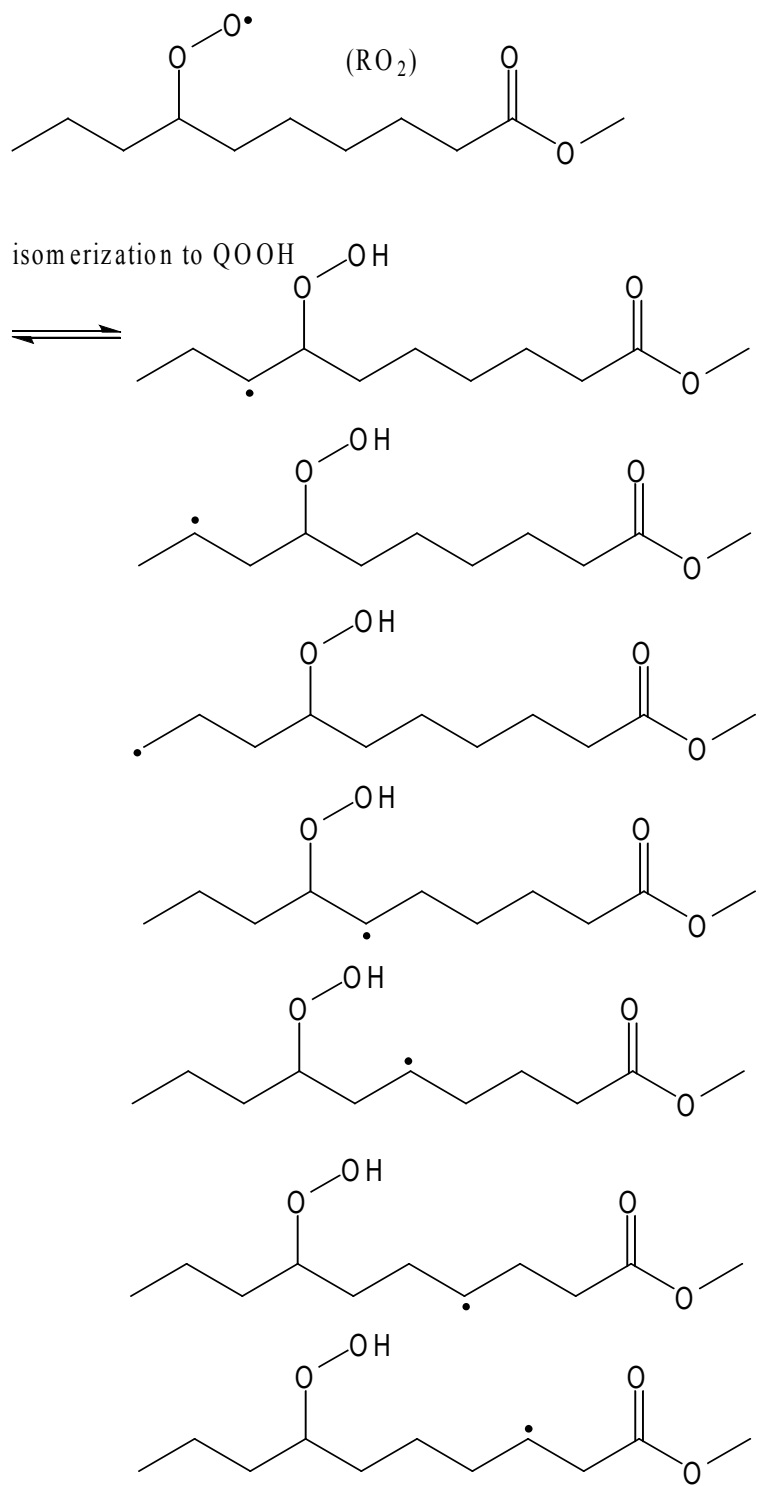Figure 4: Addition of an alkyl-ester radical (R) to O_2.

Figure 5: Examples of isomerizations permitted for peroxy alkyl-ester radicals (RO_2).
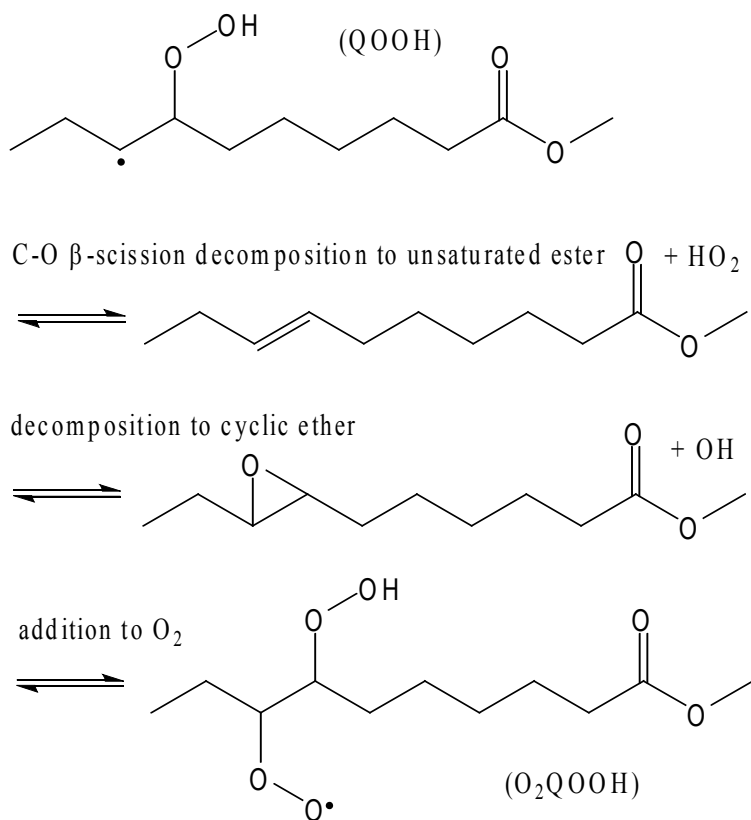
Figure 6: Reactions of an hydroperoxy ester radical (QOOH) involved in the low temperature part of the mechanism.

Figure 7: Reaction of isomerization of O_2QOOH to ketohydroperoxide + OH.

Figure 8: Comparison of the methyl decanoate model with rapeseed oil methyl ester experiments in a jet stirred reactor (P = 10 atm, ϕ = 0.5, τ = 1 s) [13].

Figure 9: Comparison of the methyl decanoate model with rapeseed oil methyl ester experiments in a jet stirred reactor (P = 10 atm, ϕ = 1, τ = 1 s) [13].

Figure 10: Comparison of the methyl decanoate − n-heptane model with rapeseed oil methyl ester experiments in a jet stirred reactor (P = 10 atm, ϕ = 0.5, τ = 1 s) [13].

Figure 11: Comparison of the methyl decanoate − n-heptane model with rapeseed oil methyl ester experiments in a jet stirred reactor (P = 10 atm, ϕ = 1, τ = 1 s) [13].

Figure 12: Mole fractions of unsaturated esters computed with the methyl decanoate model (jet stirred reactor, P = 10 atm, ϕ = 0.5, τ = 1 s).
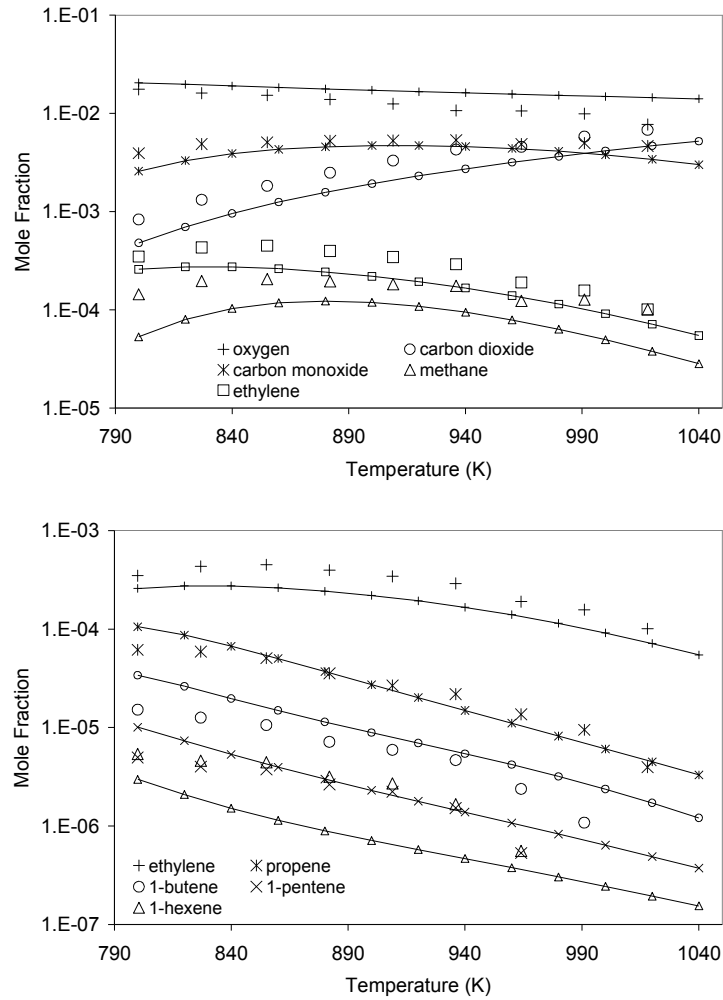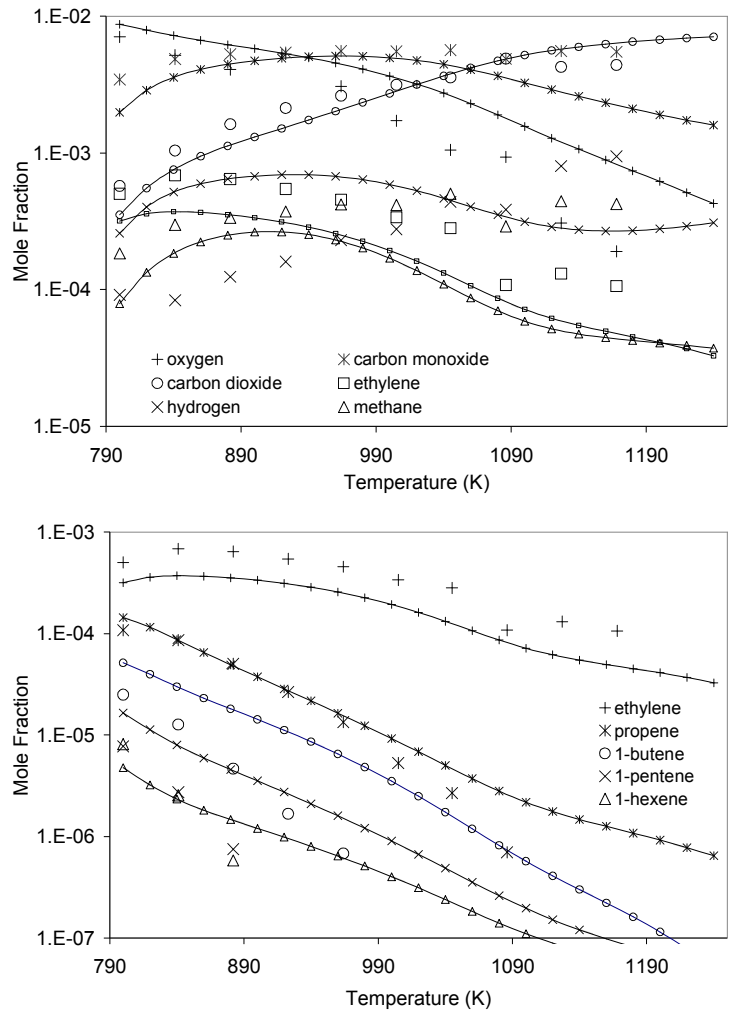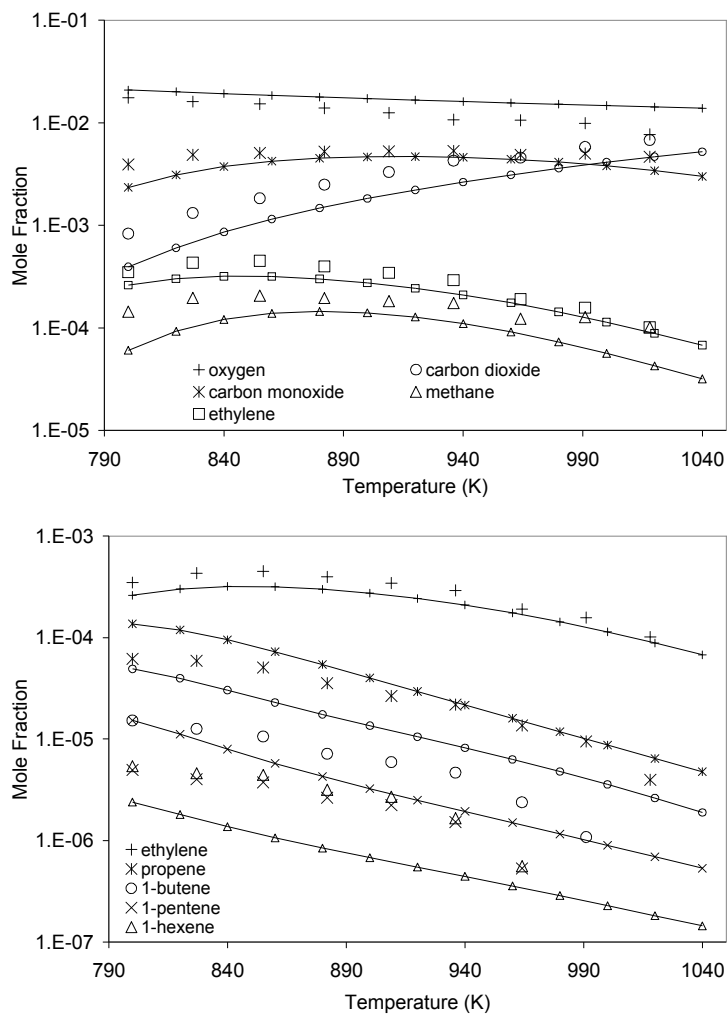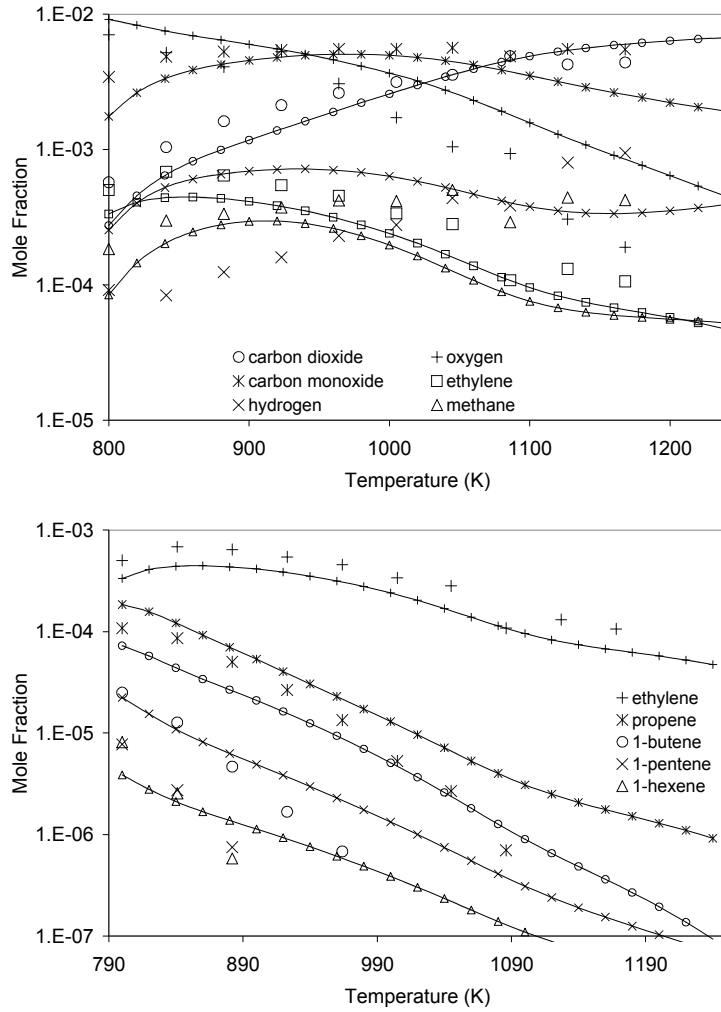
Figure 13: Successive reactions from an alkyl-ester radical to the formation of CO_2 via the radical OCHO.

Figure 14: Formation of the radical CH_3OCO from a 3-alkyl ester radical.

Figure 15: Main reactions of radicals in the low temperature region (τ = 1 s, P = 10 atm, ϕ = 0.5 and T = 800 K).

Figure 16: Reactions of isomerization of peroxy radicals in the low temperature region (τ = 1 s, P = 10 atm, ϕ = 0.5 and T = 800 K).

Figure 17: Main unimolecular initiations of the reactant in the high temperature region (τ = 1 s, P = 10 atm, ϕ = 0.5 and T = 1040 K).

Figure 18: Decomposition of an olefin, 1-hexene at high temperature (τ = 1 s, P = 10 atm, ϕ = 0.5 and T = 1040 K).

Figure 19: Comparison of fuel reactivity at 0.03% of fuel, ϕ=1, 2.15 atm, 99.505 % Ar. Line – methyl decanoate prediction. Open squares – n-decane experimental data [19].

Figure 20: OH profiles (0.03% of fuel, ϕ=1, 99.505 % Ar). Lines – methyl decanoate model predictions. Open symbols – n-decane experimental data [19].

Figure 21: Comparison of fuel reactivity under shock tube conditions, in air, ϕ=1, Lines – methyl decanoate model predictions. Open symbols – n-decane experimental data [38].

Figure 22: Gases in the residual part of the cylinder were taking in account by considering consecutive cycles.

Figure 23: Mass fractions (% of fuel C) of CO ($\diamondsuit$), CO_2 ($\triangle$), CH_2O ($\bigcirc$) and CH_3CHO ($\square$) at an equivalence ratio of 0.25 in the case of n-heptane simulations in an engine. Open symbols correspond to experiments [18] and lines to simulations.

Figure 24: Mass fractions of CO ($\diamondsuit$), CO_2 ($\triangle$), CH_2O ($\bigcirc$) and CH_3CHO ($\square$) at an equivalence ratio of 0.25. Open symbols correspond to experiments [18] and lines to simulations.

Figure 25: Decomposition by C-H bond β-scission of a 3-alkyl-ester radical.

Figure 26: Pathway for the formation of carboxylate radicals.

Figure 1: Structure of the main components found in soybean and rapeseed oils methyl esters and of methyl decanoate.

RH

R $\longrightarrow$ olefin + R

O_2

RO_2

QOOH $\longrightarrow$ olefin + HO_2
cyclic ether + OH

O_2

O_2QOOH $\longrightarrow$ keto-hydroperoxide + OH

$\longrightarrow$ (low T branching)

Figure 2: Primary oxidation reactions taken into account for the development of the

methyl decanoate mechanism.

Figure 3: Potential energy diagram for the addition of R to O_2 and subsequent reactions (low temperature scheme used in the methyl decanoate mechanism).

Figure 4: Addition of an alkyl-ester radical (R) to O_2.

Figure 5: Examples of isomerizations permitted for peroxy alkyl-ester radicals (RO_2).

Figure 6: Reactions of an hydroperoxy ester radical (QOOH) involved in the low

temperature part of the mechanism.

Figure 7: Reaction of isomerization of O_2QOOH to ketohydroperoxide + OH.

Figure 8: Comparison of the methyl decanoate model with rapeseed oil methyl ester

experiments in a jet stirred reactor (P = 10 atm, ϕ = 0.5, τ = 1 s) [13].

Figure 9: Comparison of the methyl decanoate model with rapeseed oil methyl ester

experiments in a jet stirred reactor (P = 10 atm, ϕ = 1, τ = 1 s) [13].

Figure 10: Comparison of the methyl decanoate – n-heptane model with rapeseed oil

methyl ester experiments in a jet stirred reactor (P = 10 atm, ϕ = 0.5, τ = 1 s) [13].

Figure 11: Comparison of the methyl decanoate – n-heptane model with rapeseed oil

methyl ester experiments in a jet stirred reactor (P = 10 atm, ϕ = 1, τ = 1 s) [13].

Figure 12: Mole fractions of unsaturated esters computed with the methyl decanoate

model (jet stirred reactor, P = 10 atm, ϕ = 0.5, τ = 1 s).

Figure 13: Successive reactions from an alkyl-ester radical to the formation of CO_2 via the radical OCHO.

Figure 14: Formation of the radical CH$_3$OCO from a 3-alkyl ester radical.

Figure 15: Main reactions of radicals in the low temperature region ($\tau = 1$ s, $P = 10$ atm, $\phi = 0.5$ and $T = 800$ K).

Figure 16: Reactions of isomerization of peroxy radicals in the low temperature region (τ = 1 s, P = 10 atm, ϕ = 0.5 and T = 800 K).

Figure 17: Main unimolecular initiations of the reactant in the high temperature region (τ = 1 s, P = 10 atm, ϕ = 0.5 and T = 1040 K).
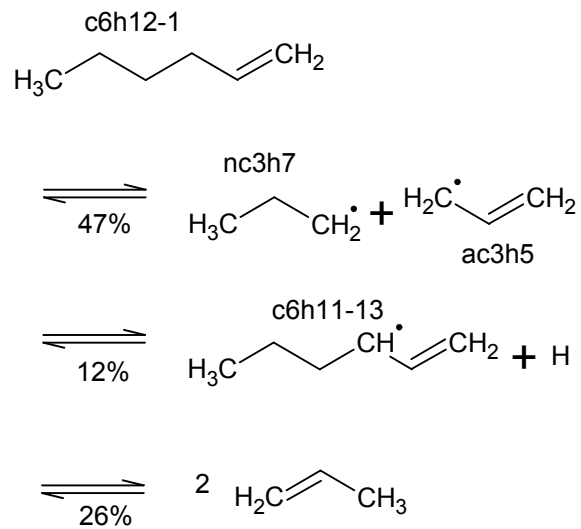
Figure 18: Decomposition of an olefin, 1-hexene at high temperature ($\tau = 1$ s, P = 10 atm, $\phi = 0.5$ and T = 1040 K).
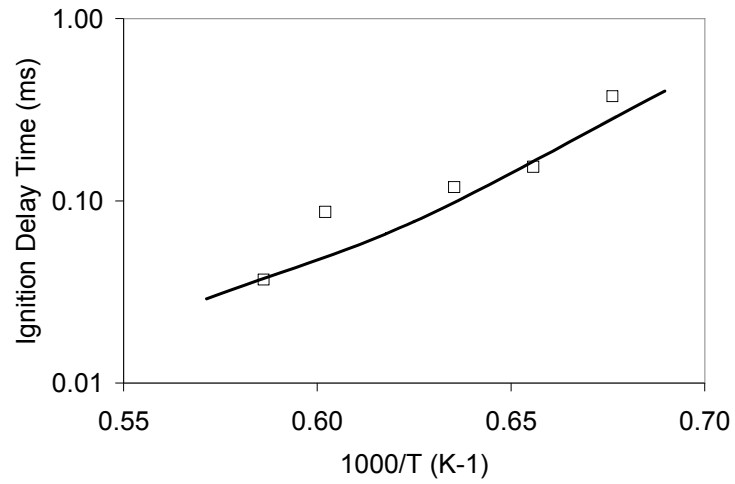
Figure 19: Comparison of fuel reactivity at 0.03% of fuel, $\phi=1$, 2.15 atm, 99.505 % Ar.

Line – methyl decanoate prediction. Open squares – n-decane experimental data [19].

Figure 20: OH profiles (0.03% of fuel, ϕ=1, 99.505 % Ar). Lines – methyl decanoate

model predictions. Open symbols – n-decane experimental data [19].

Figure 21: Comparison of fuel reactivity under shock tube conditions, in air, ϕ=1, Lines –

methyl decanoate model predictions. Open symbols – n-decane experimental data [38].

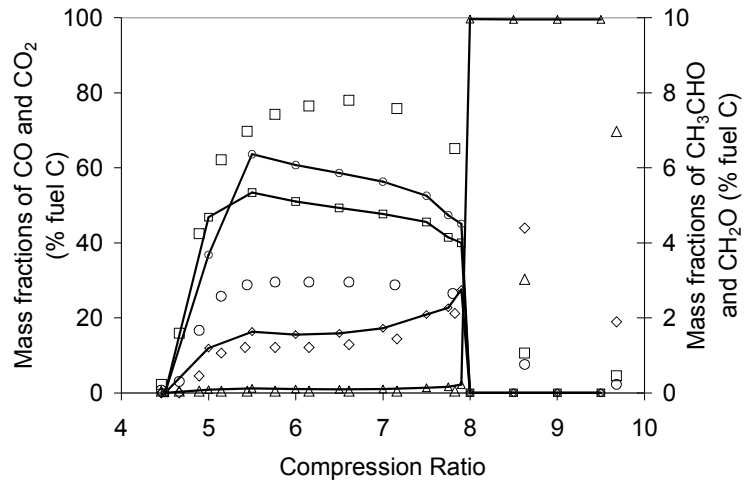Figure 22: Gases in the residual part of the cylinder were taking in account by considering consecutive cycles.

Figure 23: Mass fractions (% of fuel C) of CO ($\Diamond$), CO_2 ($\triangle$), CH_2O ($\bigcirc$) and CH_3CHO

($\square$) at an equivalence ratio of 0.25 in the case of n-heptane simulations in an engine.

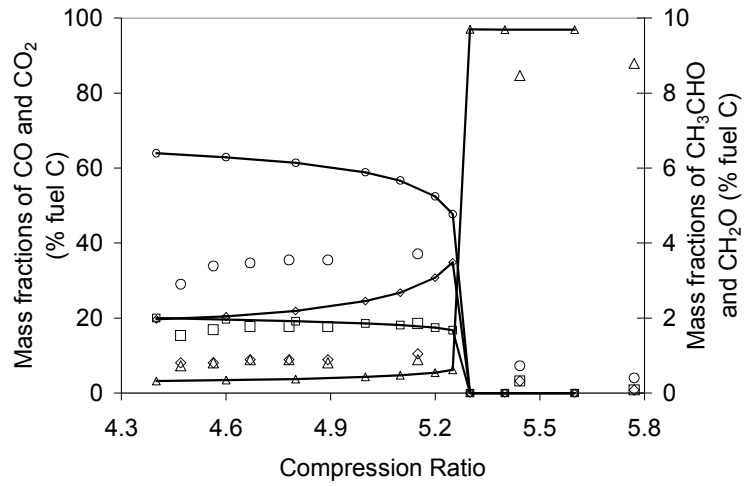Open symbols correspond to experiments [18] and lines to simulations.

Figure 24: Mass fractions of CO ($\diamond$), CO_2 ($\triangle$), CH_2O ($\bigcirc$) and CH_3CHO ($\square$) at an equivalence ratio of 0.25. Open symbols correspond to experiments [18] and lines to simulations.
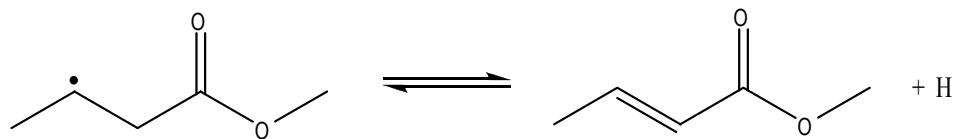
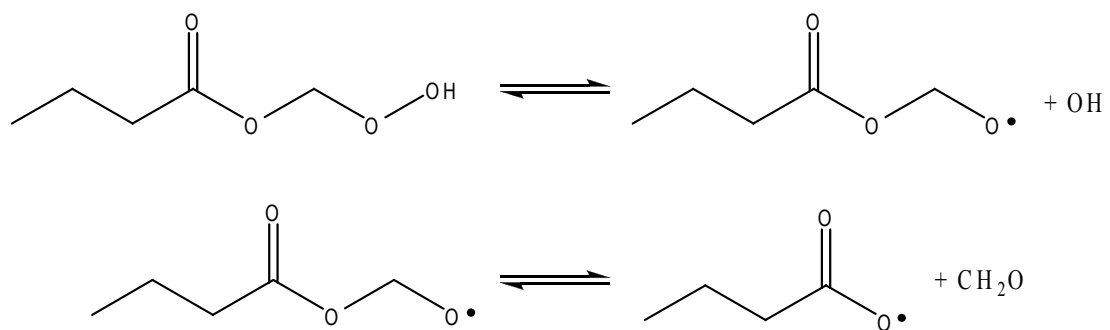Figure 25: Decomposition by C-H bond β-scission of a 3-alkyl-ester radical.

Figure 26: Pathway for the formation of carboxylate radicals.